Change in the electronic structure of the bismuth chalcogenide superconductor $CsBi_{4-x}Pb_xTe_6$ by dissociation of the bismuth dimers

Hiroyuki Okazaki,[1,2,3] Kensei Terashima,[3] David Billington,[4] Keiji Iwata,[2] Takanori Wakita,[2] Masashi Tanaka,[3,5] Yoshihiko Takano,[3] Yuji Muraoka,[2] Takayoshi Yokoya[2]

[1] Takasaki Advanced Radiation Research Institute, National Institutes for Quantum and Radiological Science and Technology, Takasaki, Gunma 370-1292, Japan

[2] Research Institute for Interdisciplinary Science (RIIS), Okayama University, Okayama 700-3537, Japan

[3] National Institute for Materials Science, 1-2-1 Sengen, Tsukuba, Ibaraki 305-0047, Japan

[4] School of Physics and Astronomy, Cardiff University, Queen's Building, The Parade, Cardiff, CF24 3AA, United Kingdom

[5]Graduate School of Engineering, Kyushu Institute of Technology, 1-1 Sensui-cho, Tobata, Kitakyushu, 804-8550, Japan

Abstract

$CsBi_{4-x}Pb_xTe_6$ is synthesized and the superconductivity associated with the structural transition from Pb substitution is studied. Photoemission spectroscopy measurements are performed in order to elucidate the relationship between the electronic structure and the occurrence of the superconductivity. When Bi is substituted with Pb, an electron doping-like change in the electronic structure is directly observed which is contrary to the naive expectation of hole doping. This observation is consistent with band structure calculations and appears to be a unique characteristic of $CsBi_{4-x}Pb_xTe_6$ because of the dissociation of Bi dimers upon Pb substitution. These results indicate that it may be possible to control the electron and hole doping via manipulating the Bi dimers through Pb substitution.

Introduction

Many reports of superconductivity in doped Mott and band insulators suggest that carrier doping can provide a platform to explore new superconducting systems. A well-known example is the cuprates which have high superconducting transition temperatures (T_c) and change from a Mott insulating state to a superconductor by carrier doping [1,2]. There are also a variety of systems in which superconductivity emerges by carrier doping parent semiconductors such as diamond [3,4], silicon [5], and so on. Indeed, many chalcogenide semiconductors such as PbTe [6], SnTe [7], Bi_2Se_3 [8], and Bi_2Te_3 [9] also exhibit superconductivity when carrier doped. Recently, it was reported that superconductivity occurs in the layered Bi-chalcogenides $LnOBi(S, Se)_2$ [10] (Ln: lanthanoid) and ABi_4Te_6 [11-13] (A: alkali metal, Cs or Rb). These Bi-chalcogenide superconductors have provoked much attention since the superconductivity occurs under strong influence of the spin-orbit interaction.

For the $LnOBi(S, Se)_2$ system, there have been many reports about the superconducting properties [14] and the electronic structure has been experimentally probed by angle-resolved photoemission spectroscopy (ARPES) [15]. The experimental band structure is in good agreement with the predictions of first-principles calculations that include spin-orbit coupling and show that the density-of-states (DOS) near the Fermi level (E_F) comes from Bi.

The ABi_4Te_6 system changes from a narrow-gap semiconductor to the superconductor by inducing either (i) Cs vacancies or (ii) off-stoichiometry in the ratio between Bi and Te, or (iii) partial substitution of Pb for Bi. Among them, the Pb substitution case ($CsBi_{4-x}Pb_xTe_6$) shows a structural change from monoclinic to orthorhombic by the dissociation of the Bi-dimers, which occurs simultaneously with the change from a semiconductor (filamentary superconductor) to a bulk superconductor [12]. Such an emergence of superconductivity accompanied with a structural transition is reminiscent of the Fe-base superconductor $CaFe_2(As_{1-x}P_x)_2$, where a first-order structural transition leads to a change of a hole-like Fermi surface and influences the superconductivity due to the existence or non-existence of As-As bonding in that system. Therefore, understanding the correlation between the Bi-dimers and the superconductivity in the $CsBi_{4-x}Pb_xTe_6$ system via a study

of the electronic states would be worthwhile. However, XANES and XPS studies [16] on $CsBi_{4-x}Pb_xTe_6$ (x = 0 and 0.5) are scarce, and the valence band structure of the $ABi_{4-x}Pb_xTe_6$ superconductor has not yet been experimentally determined. It is, therefore, crucial to study the experimental valence band of stoichiometric $CsBi_4Te_6$ and its evolution with Pb substitution in order to understand the occurrence of bulk superconductivity in $CsBi_{4-x}Pb_xTe_6$. This study might shed light on the mechanism of Bi-based superconductivity since the Pb substitution affects the crystal and electronic structures, and the superconductivity.

Here we study the relationship between the crystal structure, the valence band, and the superconductivity in the $CsBi_{4-x}Pb_xTe_6$ system. The compounds are synthesized and the emergence of superconductivity associated with a structural transition due to the Pb substitution is observed. We also observed the change in the electronic structures in the valence band of $CsBi_{4-x}Pb_xTe_6$ across the Pb-substitution induced structural transition. From a comparison between the experimental results and band structure calculations, it was found that the valence band near E_F is mainly comprised of Bi and Te orbitals. From the comparison with other Bi-based superconductors, we demonstrate that $CsBi_{4-x}Pb_xTe_6$ has unique doping characteristics among the bismuth-chalcogenide compounds due to the Bi dimers.

Experimental

$CsBi_4Te_6$ samples were prepared by a reaction between Bi_2Te_3 powder and a small excess (~1 %) of Cs, as explained in ref. [11]. These chemicals were mixed in alumina cells in a glovebox and then the alumina cells were sealed into an evacuated quartz ampoule. The sealed materials were heated at 700 °C for 50 hours and then cooled by air-quenching to room temperature. $CsBi_{4-x}Pb_xTe_6$ samples were synthesized by reacting Bi_2Te_3, Te, Pb, and a small excess Cs in two steps. In the first step, the mixture is heated at 700 °C for 30 hours, followed by furnace cooling. For the second step, the products are heated at 700 °C for 12 hours and then air-quenched to room temperature.

Powder X-ray diffraction measurements were performed on powdered samples. XRD profiles

were collected at ambient temperature by Rigaku Miniflex with a wavelength of λ = 1.54056 Å in a glovebox filled with N_2 gas. We also confirmed its T_c from magnetic susceptibility measurements using a superconducting quantum interface device (SQUID, Quantum Design). Photoemission spectroscopy measurements were performed at Okayama University on a spectrometer built with a Scienta Omicron R4000 electron analyzer. The spectra were measured at 20 K under vacuum with pressures below 3×10^{-8} Pa using the He Iα (21.2 eV) resonance line. The total energy resolution was set to 30 meV for the valence band spectra and 15 meV for the spectra near E_F, respectively. E_F of the sample was referenced to that of a gold film, which was measured frequently during the experiments. The samples were cleaved under ultra-high vacuum in order to measure a clean surface.

The ground-state electronic structures of monoclinic $CsBi_4Te_6$ and orthorhombic $CsPb_xBi_{4-x}Te_6$ (x = 0.3) were calculated from first principles with the ELK code [17], a highly-accurate full-potential augmented plane-wave plus local orbital (FP-APW+lo) method. The experimentally determined crystal structures of Hsu *et al*. (space group *C*2/*m* for monoclinic $CsBi_4Te_6$ and *Cmcm* for orthorhombic $CsPb_xBi_{4-x}Te_6$ (x = 0.3)) were used [18]. For monoclinic $CsBi_4Te_6$, convergence was achieved with a 16 × 8 × 4 *k*-point grid and a plane-wave cut-off in the interstitial region of $|G + k|_{max} = 8.5/R_{mt}$ (where R_{mt} is the average muffin-tin radius). For orthorhombic $CsPb_xBi_{4-x}Te_6$ (x = 0.3), convergence was achieved with a 16 × 16 × 8 *k*-point grid and the same $|G + k|_{max} = 8.5/R_{mt}$. For both monoclinic $CsBi_4Te_6$ and orthorhombic $CsPb_xBi_{4-x}Te_6$ (x = 0.3), the muffin-tin radii for Cs, (Pb,Bi) and Te were 2.8, 2.8 and 2.6 a.u., respectively. For the exchange-correlation functional, the Perdew-Burke-Ernzerhof generalised gradient approximation (PBE-GGA) [19] was used. Since Cs, (Pb,Bi) and Te are all heavy atoms, the spin-orbit interaction was included in the calculations by adding a term of the form $\boldsymbol{\sigma} \cdot \mathbf{L}$ (where $\boldsymbol{\sigma}$ is the spin vector and $\boldsymbol{L}$ is the orbital angular momentum vector) to the second variational Hamiltonian.

Results and discussion

We first characterized the crystal structure of our $CsBi_{4-x}Pb_xTe_6$ samples by X-ray diffraction

measurements. Figure 1(a) shows the experimental diffraction profiles for the samples with nominal compositions of $x = 0$, and 0.3, respectively. The $CsBi_4Te_6$ shows a monoclinic structure ($C2/m$) with a = 51.927(4) Å, b = 4.4561(5) Å, c = 14.4550(9) Å, and β = 101.536(5)°. These parameters are similar to those reported previously [20]. As seen in Fig. 1, the XRD profiles show the structural transition by Pb-substitution, as shown in a previous report [12], indicating that the crystal structure evidently changes from monoclinic to orthorhombic [18]. Orthorhombic $CsBi_{3.7}Pb_{0.3}Te_6$ has lattice parameters of a = 6.3685(7) Å, b = 28.438(3) Å, c = 4.3886(7) Å. The illustrations of both structures are shown in Fig. 1(b). The prominent difference between those structures is the existence/disappearance of Bi dimers [20]. Namely, $CsBi_4Te_6$ has Bi dimers near the center and at both ends of the cell shown in the figure, but $CsBi_{3.7}Pb_{0.3}Te_6$ does not. The disconnection of the Bi-Bi bonding results in the higher-symmetry structure of $CsBi_{4-x}Pb_xTe_6$ (which only has Bi-Te bonds) than that of $CsBi_4Te_6$. We also confirmed the superconductivity in $CsBi_{4-x}Pb_xTe_6$ from the temperature dependence of magnetic susceptibility in an applied field of 10 Oe. A diamagnetic signal is observed at 2.9 K in $CsBi_{3.7}Pb_{0.3}Te_6$, as shown in Fig. 2.

Next, we performed photoemission spectroscopy in order to elucidate how the electronic structure changes with Pb substitution. Figure 3 shows the photoemission spectra of $CsBi_{4-x}Pb_xTe_6$. The spectrum of $CsBi_4Te_6$ shows almost no intensity at E_F, indicating that $CsBi_4Te_6$ has a band gap at E_F. This is consistent with the results of the temperature dependence of the resistivity [12,20]. We observed characteristic peak structures in the $CsBi_4Te_6$ spectrum, labelled as A and B in Fig. 3. We compared the spectrum with band structure calculations of $CsBi_4Te_6$ [21]. The calculated density of states (DOS) shows a good correspondence with our spectral shape. Thus, we found that the experimental valence band reflects the bulk electronic structure of $CsBi_4Te_6$. According to the band calculation, the valence band between E_F and binding energies of 5 eV is mainly composed of the hybridized states of Bi 6*p* and Te 5*p*.

As shown in Fig. 3(b), the spectral shape of $CsBi_{3.7}Pb_{0.3}Te_6$ is clearly different from that of $CsBi_4Te_6$. We observed one main peak D and small peaks C and E. The small peak E stays at the

almost same energy as peak B in $CsBi_4Te_6$. Additionally, the valence band spectrum of $CsBi_{3.7}Pb_{0.3}Te_6$ exhibits only one main peak D at 1.8 eV while $CsBi_4Te_6$ shows a two peaks structure around A between 1 and 2 eV. These results indicate that the valence band structure is modulated by the change of the crystal structure through the Pb substitution. For $CsBi_{3.7}Pb_{0.3}Te_6$, there are two important points to note about the new feature C with a peak position of around 0.2 eV: (1) The new feature C exhibits a clear Fermi edge, as shown in Fig. 3(c), indicating that this system changes from a semiconducting to a metallic state. (2) Provided that features D and E correspond to features A and B, respectively, the energy positions of D and E are slightly shifted to lower binding energy, as if the Pb substitution leads to electron doping. Thus, the structure C is considered to be the bottom of conduction band in this system. This is an interesting observation because the Pb substitution into Bi site normally results in hole doping.

Here it is essential to compare the experimental results with the density of states derived by band structure calculation in order to discuss the effect of the Pb substitution. For $CsBi_4Te_6$, the experimental valence band is very similar to that from the band structure calculation, as shown in Fig. 4(a). According to the calculation, the partial density of states (pDOS) of Te dominates the two peaks A in Fig. 3. On the other hand, the peak B in Fig. 3 is characterized by pDOS of both Bi and Te. The top of valence band consists primarily of the Te pDOS with a small contribution from the Bi pDOS. In the bottom of the conduction band, the orbital contributions from Bi and Te are comparable. Focusing on the DOS of the Bi dimers, the contribution of the Bi pDOS to the top of the valence band is large in spite of coming from just two of the eight Bi sites in the unit cell, as shown in Fig. 4(b). Figure 4(c) shows the comparison of the valence band spectrum with the calculation for $CsBi_{3.7}Pb_{0.3}Te_6$. It is clear from the figure that the overall spectral shape in $CsBi_{3.7}Pb_{0.3}Te_6$ is also well reproduced by the calculation. Based on the comparison with the calculated results, we identify the main peak in the spectrum of $CsBi_{3.7}Pb_{0.3}Te_6$ around 1.5 eV (D in Fig. 3) is dominated by the pDOS of Te. We also found that the peak around 4 eV (E in Fig. 3) consists of the pDOS from both Bi and Te. The calculation ensures our previous assignment of the peaks in two compounds, namely the peak

structure A in $CsBi_4Te_6$ corresponds to D in $CsBi_{3.7}Pb_{0.3}Te_6$ and peak B in $CsBi_4Te_6$ corresponds to E in $CsBi_{3.7}Pb_{0.3}Te_6$. Regarding the calculated DOS of $CsBi_4Te_6$ and $CsBi_{3.7}Pb_{0.3}Te_6$, the overall shape is almost the same each other, however, the DOS is rigidly shifted toward higher binding energies in $CsBi_{3.7}Pb_{0.3}Te_6$, which is indicative of electron doping and is consistent with our experimental observation. Therefore, Pb substitution indeed results in the electron-like doping for this system although one expects the substitution of $_{82}$Pb for $_{83}$Bi would induce hole doping.

Figure 5 shows illustrates the changes in the crystal and electronic structure caused by Pb-substitution. For stoichiometric $CsBi_4Te_6$, the Bi dimer connects the Bi-Te networks in the crystal structure. Since the Bi dimer captures an electron provided by an intercalated Cs atom [15,22], $CsBi_4Te_6$ has semiconducting character although the electrons from the alkali metals are doped in the parent insulating Bi_4Te_6. For $CsBi_{4-x}Pb_xTe_6$, the Bi dimer gets disconnected by the Pb substitution and then the doped electrons originating from Cs move into the Bi-Te network. The partial substitution of Pb for Bi generally leads to hole doping, but in $CsBi_{4-x}Pb_xTe_6$ this results in electron doping of the Bi_4Te_6 network because of the disappearance of the Bi dimer. H. Chen *et al*. have demonstrated that the carrier type depends on the crystal structure (monoclinic or orthorhombic structure) [23]. Thus, the Bi_4Te_6 system whose carriers can be controlled by the Bi dimer provides a unique playground to study superconductivity in bismuth-chalcogenide compounds. For the case of hole doping into this system ($Cs_{1-x}Bi_4Te_6$), even though the Bi dimer remains, the system exhibits a superconducting transition around 4 K, although the shielding volume fraction has remained relatively low (~10%) so far [11]. On the other hand, $CsBi_{4-x}Pb_xTe_6$ system without Bi dimer shows the shielding volume fraction of about 100%. Since the EXAFS research reported that the Bi dimer distorts the Bi_4Te_6 layers [16], destabilized regions could exist at grain boundaries and the $CsBi_4Te_6$ system might exhibit filamentary superconductivity. On the other hand, $CsBi_{4-x}Pb_xTe_6$ probably exhibits bulk superconductivity because the Pb-substitution leads to the $CsBi_{4-x}Pb_xTe_6$ crystal becoming more uniform.

It is also fruitful to compare our results with other Bi-based superconductors. Here we compare

with the $LnO_{1-x}F_xBiS_2$ superconductor because $LnO_{1-x}F_xBiS_2$ also has Bi-chalcogen bonds and a layered structure as in $CsBi_{4-x}Pb_xTe_6$. According to band structure calculations of $LnO_{1-x}F_xBiS_2$ [24], $LaOBiS_2$ exhibits an insulating state with a band gap of 0.8 eV. The pDOS due to the Bi orbitals dominates the bottom of the conduction band rather than the S orbitals which dominate the top of the valence band. It has been reported from photoemission spectroscopy that this system shows a rigid shift of the band structure relative to E_F by electron doping due to the addition of F [25]. Thus, the conduction electrons from the dominant Bi orbitals contribute to the superconductivity in $LnO_{1-x}F_xBiS_2$ [25]. These features are very different from $CsBi_{4-x}Pb_xTe_6$ system because the $CsBi_{4-x}Pb_xTe_6$ system has a mixed DOS of Bi and Te orbitals in the vicinity of E_F. In the bismuth chalcogenide superconductors, the comparable pDOS from Bi and Te in the Bi_4Te_6 system is similar to Bi_2Te_3 [26]. It is worth noting that the BiS_2 system shows slightly higher transition temperature (maximum of about 5K) than the $CsBi_{4-x}Pb_xTe_6$ system (about 3 K). Other block layers should be studied in Bi_4Te_6-based systems as has been done for $LnO_{1-x}F_xBiS_2$ because other block layers may result in a higher T_c than that of the BiS_2 system. Indeed, it has been reported that T_c slightly increases for the other block layers of Na and K [25]. Further studies might elucidate the relationship between the contribution of the Bi orbitals and the superconducting T_c for the bismuth-chalcogenide superconductors.

Conclusion

Photoemission spectroscopy was performed on $CsBi_{4-x}Pb_xTe_6$ (x = 0.0 and 0.3). This system exhibits a Pb-substitution induced semiconductor (filamentary superconductive) to metal (bulk superconductive) transition, accompanied with a structural change due to Bi-dimer disconnection. The photoemission spectrum of $CsBi_{3.7}Pb_{0.3}Te_6$ shows new states with a metallic edge near the Fermi level (E_F), consistent with the semiconductor to metal transition, and an energy shift of main valence band structure to higher binding energy compared to those of $CsBi_4Te_6$, and this observation is consistent with band structure calculations. The observed “electron-doping-like” behavior, regardless

of the expected hole doping due to Pb substitution for Bi, can be explained by a scenario in which part of the Cs 6*s* electrons occupying the bonding state of the Bi dimer in $CsBi_4Te_6$ instead occupy the conduction band of $CsBi_{3.7}Pb_{0.3}Te_6$ after the disconnection of Bi dimer due to the Pb-substitution. Therefore, we clearly demonstrate that the charge carriers can be controlled by the Bi dimers in the Bi_4Te_6 system and this provides unique playground to study superconductivity in bismuth-chalcogenide compounds.

Acknowledgements

Calculations were performed using the computational facilities of the Advanced Computing Research Centre, University of Bristol, UK (http://www.bris.ac.uk/acrc/). This work was supported partly by a Grant-in-Aid for Scientific Research of the Ministry of Education, Culture, Sports, Science and Technology, Japan.

Reference

[1] J. G. Bednorz and K.A. Műller, Z. Phys. B **64**, 189 (1986).

[2] H. Maeda, Y. Tanaka, M. Fukutomi, and T. Asano, Jpn. J. Appl. Phys. **27**, L209 (1988).

[3] Y. Takano, M. Nagao, T. Takenouchi, H. Umezawa, I. Sakaguchi, M. Tachiki, and H. Kawarada, Diamond Relat. Mater. **14**, 1936 (2005).

[4] H. Okazaki, T. Wakita, T. Muro, T. Nakamura, Y. Muraoka, T. Yokoya, S. Kurihara, H. Kawarada, T. Oguchi, and Y. Takano, Appl. Phys. Lett. **106**, 052601 (2015).

[5] E. Bustarret, C. Marcenat, P. Achatz, J. Kačmarčik, F. Lévy, A. Huxley, L. Ortéga, E. Bourgeois, X. Blase, D. Débarre, and J. Boulmer, Nature **444**, 465 (2006).

[6] B. Lalevic, Phys. Lett. **16**, 206 (1965).

[7] R. A. Hein and P. H. E. Meijer, Phys. Rev. **179**, 497 (1969).

[8] Y. S. Hor, A. J. Williams, J. G. Checkelsky, P. Roushan, J. Seo, Q. Xu, H. W. Zandbergen, A. Yazdani, N. P. Ong, and R. J. Cava, Phys. Rev. Lett. **104**, 057001 (2010).

[9] M. Einaga, Y. Tanabe, A. Nakayama, A. Ohmura, F. Ishikawa, and Y. Yamada, J. Phys. Conference Series **215**, 012036 (2010).

[10] Y. Mizuguchi, S. Demura, K. Deguchi, Y. Takano, H. Fujihisa, Y. Gotoh, H. Izawa, and O. Miura, J. Phys. Soc. Jpn. **81**, 114725 (2012).

[11] C. D. Malliakas, D. Y. Chung, H. Claus, and M. G. Kanatzidis, J. Am. Chem. Soc. **135**, 14540 (2013).

[12] R. X. Zhang, H. X. Yang, H. F. Tian, G. F. Chen, S. L. Wu, L. L. Wei, and J. Q. Li, J. Solid State Chem. **232**, 50 (2015).

[13] C. D. Malliakas, D. Y. Chung, H. Claus, and M. G. Kanatzidis, J. Am. Chem. Soc. 138, 14694 (2016).

[14] S. Demura, K. Deguchi, Y. Mizuguchi, K. Sato, Ryota Honjyo, A. Yamashita, T. Yamaki, H. Hara, T. Watanabe, S. J. Denholme, M. Fujioka, H. Okazaki, T. Ozaki, O. Miura, T. Yamaguchi, H. Takeya, and Y. Takano, J. Phys. Soc. Jpn. **84**, 024709 (2015).

[15] K. Terashima, J. Sonoyama, T Wakita, M. Sunagawa, K. Ono, H. Kumigashira, T. Muro, M. Nagao, S Watauchi, I. Tanaka, H. Okazaki, Y. Takano, O. Miura, Y. Mizuguchi, H. Usui, K. Suzuki, K. Kuroki, Y. Muraoka, and T. Yokoya, Phys. Rev. B **90**, 220512 (2014).

[16] T. Wakita, E. Paris, T. Mizokawa, M. Y. Hacisalihoğlu, K. Terashima, H. Okazaki, O. Proux, I. Kieffer, E. Lahera, W. D. Net, L. Olivi, Y. Takano, Y. Muraoka, T. Yokoya, and Na. L. Saini, Phys. Chem. Chem. Phys., **18**, 25136 (2016).

[17] The ELK FP-LAPW Code, http://elk.sourceforge.net, version 4.3.6.

[18] K.-F. Hsu, D.-Y. Chung, S. Lal, A. Mrotzek, T. Kyratsi, T. Hogan, and M. G. Kanatzidis, J. Am. Chem. Soc. **124**, 2410 (2002).

[19] J. P. Perdew, K. Burke, and M. Ernzerhof, Phys. Rev. Lett. **77**, 3865 (1996).

[20] D.-Y. Chung, T. Hogan, P. Brazis, M. R.-Lane, C. Kannewurf, M. Bastea, C. Uher, and M. G. Kanatzidis, Science **287**, 1024 (2000).

[21] K.-F. Hsu, D.-Y. Chung, S. Lal, A. Mrotzek, T. Kyratsi, T. Hogan, and M. G. Kanatzidis, J. Am. Chem. Soc. **124**, 2410 (2002).

[22] D.-Y. Chung, T. Hogan, P. Brazis, M. Rocci-Lane, C. Kannewurf, M. Bastea, C. Uher, and M. G. Kanatzidis1, Science 287, 1024 (2000).

[23] W. Luo, J. S. Almeida, J. M. Osorio-Guillen, and R. Ahuja, J. Phys. Chem. Solids **69**, 2274 (2008).

[24] P. Larson, S. D. Mahanti, D.-Y. Chung, and M. G. Kanatzidis, Phys. Rev. B 65, 045205 (2002).

[25] H. Chen, H. Claus, J.-K. Bao, C. C. Stoumpos, D. Y. Chung, W.-K. Kwok, and M. G. Kanatzidis, Chem. Mater. 30, 5293 (2018).

[26] B. Li, Z. W. Xing, and G. Q. Huang, EPL **101**, 47002 (2013).

[27] S. Nagira, J. Sonoyama, T. Wakita, M. Sunagawa, Y. Izumi, T. Muro, H. Kumigashira, M. Oshima, K. Deguchi, H. Okazaki, Y. Takano, O. Miura, Y. Mizuguchi, K. Suzuki, H. Usui, K. Kuroki, K Okada, Y. Muraoka, and T. Yokoya, J. Phys. Soc. Jpn. **83**, 033703 (2014).

[28] P. Larson, S. D. Mahanti, and M. G. Kanatzidis, Phys. Rev. B **61**, 8162 (2000).

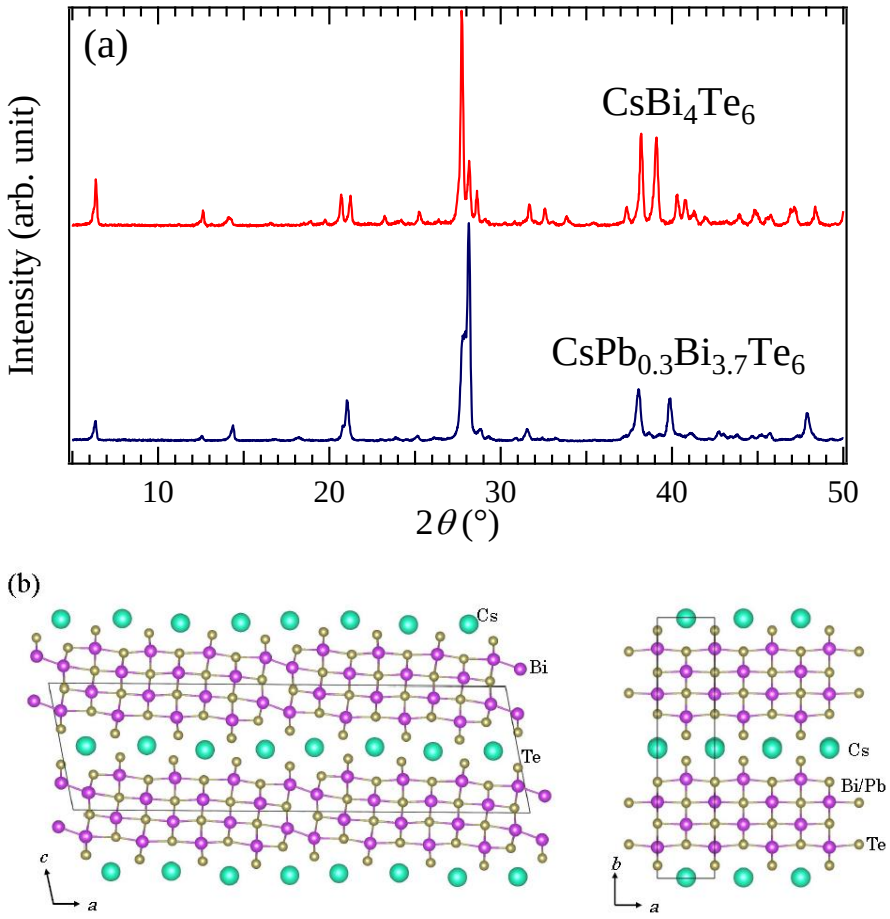

Figure 1 (a) XRD profiles of $CsBi_{4-x}Pb_xTe_6$ measured by Cu Kα radiation. The upper and lower profiles are indicated as $CsBi_4Te_6$ and $CsBi_{3.7}Pb_{0.3}Te_6$, respectively. (b) Crystal structure of $CsBi_4Te_6$ (left) and $CsBi_{3.7}Pb_{0.3}Te_6$ (right).

H. Okazaki

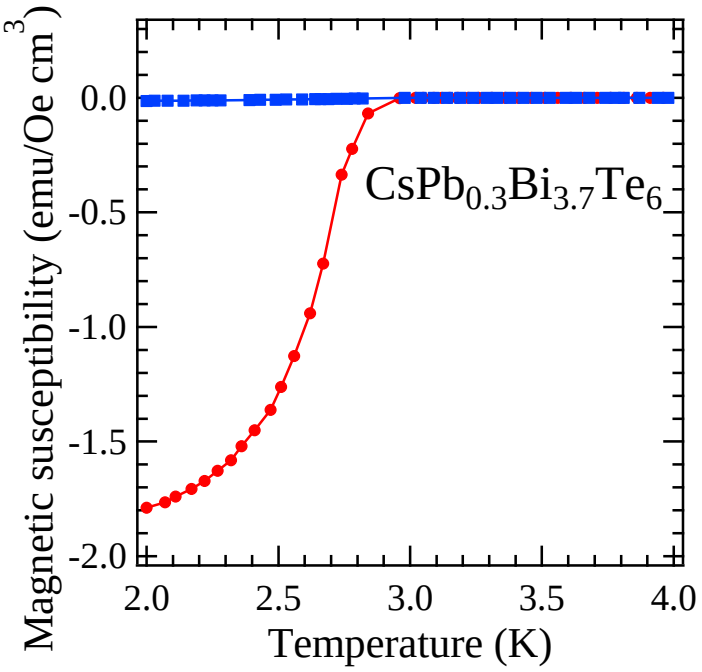

Figure 2 The temperature dependence of magnetic susceptibility for the $CsBi_{3.7}Pb_{0.3}Te_6$ sample.

H. Okazaki

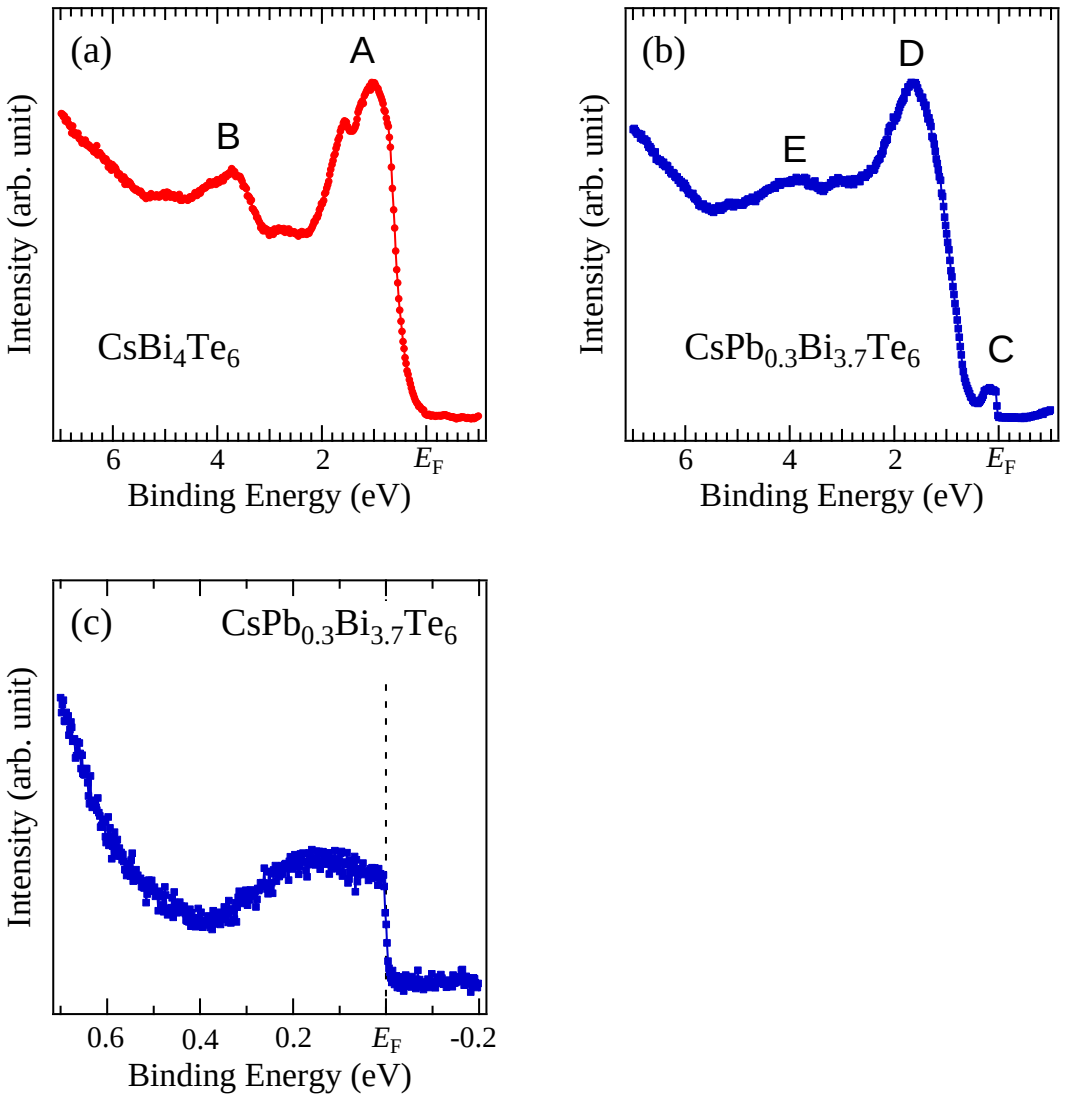

Figure 3 Photoemission spectra of (a) $CsBi_4Te_6$ and (b) $CsBi_{3.7}Pb_{0.3}Te_6$. (c) The spectrum near E_F for $CsBi_{3.7}Pb_{0.3}Te_6$.

H. Okazaki

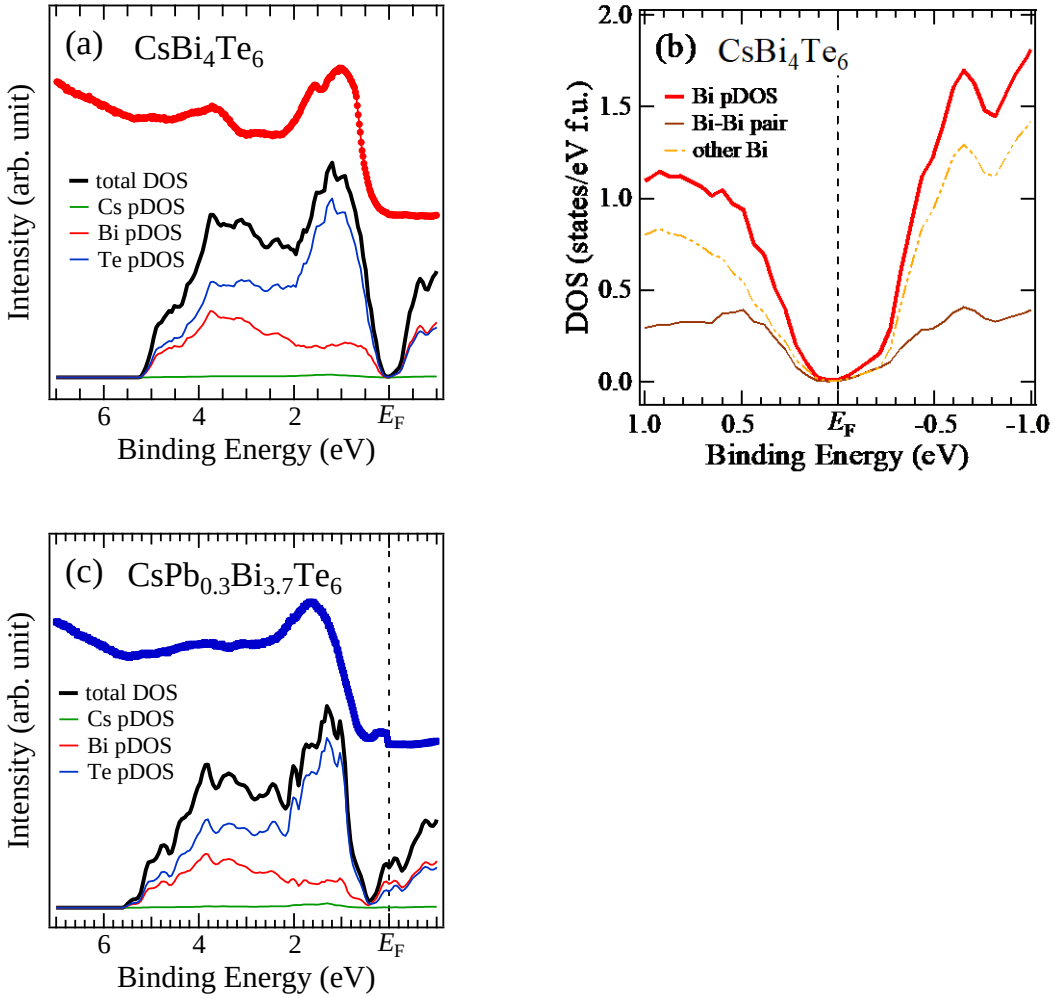

Figure 4 (a) Comparison of experimental spectra with the band calculations for $CsBi_4Te_6$. The colored lines denote as total DOS (black), pDOS of Bi (red), Te (blue), and Cs (green), respectively. (b) Calculated Bi pDOS for $CsBi_4Te_6$. (c) The comparison of experimental spectra with the band calculations for $CsPb_{0.3}Bi_{3.7}Te_6$.

H. Okazaki

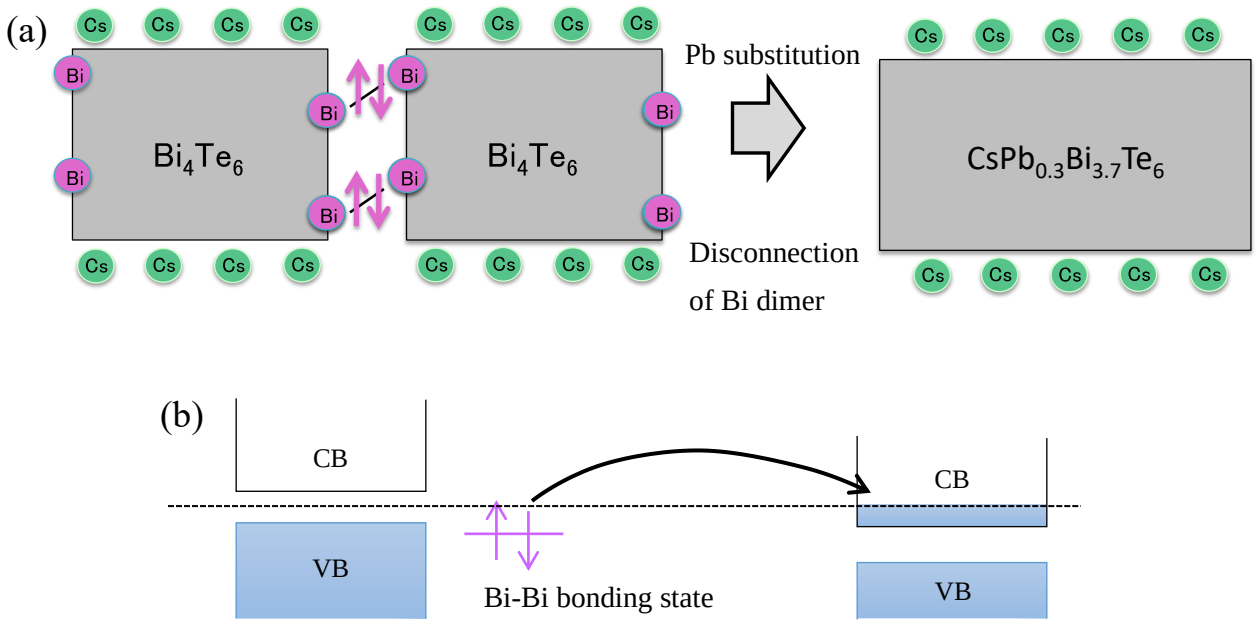

Figure 5 Schematic diagram of (a) crystal structure and (b) electronic structure for $CsBi_4Te_6$ (left) and $CsBi_{3.7}Pb_{0.3}Te_6$ (right). For $CsBi_4Te_6$, the Bi dimer connects the Bi-Te networks (slabs). For $CsBi_{3.7}Pb_{0.3}Te_6$, there is a (Bi,Pb)-Te network in the structure.